11th Asia-Pacific Conference on Combustion,
The University of Sydney, NSW Australia
10th -14th December 2017.

A Tomographic Background-Oriented Schieren Method for 3D Density Field Measurements in Heated Jets

C. Atkinson[1], S. Amjad[1], J. Soria[1,2]

[1] Laboratory for Turbulence Research in Aerospace and Combustion,
Department of Mechanical and Aerospace Engineering
Monash University, Victoria, 3800, Australia
[2] Department of Aeronautical Engineering, King Abdulaziz University,
Jeddah, Kingdom of Saudi Arabia

Abstract

Methodologies for the experimental measurement of three-dimensional instantaneous density fluctuations via tomographic background-oriented schlieren (TBOS) were assessed using synthetic background images, corresponding to experimental measurements of a heated turbulent jet. Filtered back projection and iterative algebraic reconstruction algorithms were explored. Results show a superior reconstruction when the solutions from filtered back projection were used as an initial solution to a masked and windowed iterative algebraic reconstruction. The influence of the number of cameras and the wavelength of density fluctuations are both investigated.

1 Introduction

To understand the structure of complex convective flows, it is essential to capture not only the velocity field but also the corresponding instantaneous density or temperature fields. Laser based optical measurement techniques, such as holographic or tomographic particle image velocimetry (PIV), are capable of quantifying instantaneous three-component three-dimensional (3C-3D) velocity fields [1,2], however the robust 3D measurement of density is less common. One means of quantifying the density of a flow is via an optical simplification to schlieren, known as background-oriented schlieren [3], which provides a measure of the integrated density gradients through a flow. To obtain the density gradients at discrete locations in the flow and hence enable the calculation of the density field, the distribution of density gradients along the integrated measurement must be determined. This represents an inverse Radon transform and if multiple projections of the integrated density gradients are available, corresponds to a tomographic reconstruction of the density gradient fields.

A handful of research groups report instantaneous 3D density measurements based on tomographic background-oriented schlieren (TBOS) [4,5], most using either a filtered back projection (FBP) [6] or an iterative algebraic reconstruction technique (ART) [7] to reconstruct the gradients of refractive index, which are related to the density gradients by the Gladstone-Dale relation. The validation of these approaches has generally been based on comparison with qualitative schlieren measurements, comparison of mean temperature fields or via the generation of synthetic background displacements based on density field data computed by Reynolds Averaged Navier-Stokes (RANS) simulations of specific flows.

In this paper we present and compare both FBP, ART and hybrid reconstruction techniques, combined with a random access iterative windowed and masked corrections, in order to enable the reconstruction of instantaneous 3D turbulent multi-scale density fields from simultaneous background-oriented schlieren projections. The ability of the TBOS technique to reconstruct these density fluctuations is assessed as a function of camera number and wavelength in order to aide in the planning of experimental measurements.

2 Principles of Background-Oriented Schlieren

Background-oriented schlieren (BOS) operates on the principles of a schlieren method and the relationship between the density of a fluid ρ and its refractive index n, as given by the Gladstone-Dale equation:

$$n - 1 = G(\lambda)\rho \qquad (1)$$

where $G(\lambda)$ represents the Gladstone-Dale constant as a function of the wavelength λ of the incident light. If we consider the path followed by a light ray from a point in the image plane of a camera X_o to a point in the background pattern P_o (see Fig. 1), the variation in the refractive index along this path will result in the deflection of this ray due to refraction. If the volume is small with respect to the distance to the background Z_D then it can be assumed that the path followed by the ray remains unchanged and the refracted ray can be approximated by a small deflection of angle ε, with respect to the incident ray. If a background is placed behind the measurement volume then this deflection results in an apparent shift in the imaged background $X_o + \Delta X$, which is related to the deflection and optical setup as:

$$\Delta \mathbf{X} = f\left(\frac{Z_D}{Z_D + Z_A - f}\right)\varepsilon \qquad (2)$$

where f is the focal length of the camera lens and Z_A the distance from the focal point to the centre of the measurement volume.

Corresponding author.
E-mail address: callum.atkinson@monash.edu

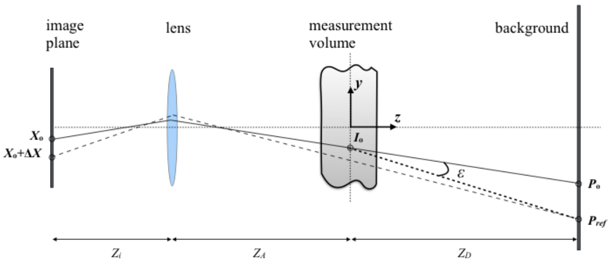

Figure 1: Schematic of the optical setup and parameters of BOS

For small angles, following the parallax assumption, the relative deflection associated with the diffraction of the ray relative to its incident angle can be approximated by:

$$\varepsilon_{z'} = \frac{1}{n_o}\int \frac{\partial n}{\partial y'}\,\mathrm{d}x' \qquad \varepsilon_{y'} = \frac{1}{n_o}\int \frac{\partial n}{\partial z'}\,\mathrm{d}x' \tag{3}$$

where $\boldsymbol{x'}$ represents the axis of the ray and $\boldsymbol{y'}$ and $\boldsymbol{z'}$ represent two axes orthogonal to the ray. The deflection angles between the ray $\boldsymbol{x'} = I_oP_o$ and $\boldsymbol{r} = I_oP_{\mathrm{ref}}$ can be determined by projecting rays from a point in the image X_o and from the point corresponding to the deflection of the background image $X_o + \Delta X$, which can be determined by standard cross-correlation particle image velocimetry algorithms. Assuming a small angle approximation, the deflections angles are given by the dot product of the local incident ray axes and the refracted ray $\boldsymbol{r}$:

$$\varepsilon_{x'} = \mathbf{r}\cdot\mathbf{x}', \quad \varepsilon_{y'} = \mathbf{r}\cdot\mathbf{y}', \quad \varepsilon_{z'} = \mathbf{r}\cdot\mathbf{z}'. \tag{4}$$

3 Tomographic BOS Reconstruction

In the present paper, tomographic reconstruction of the refractive index gradient fields $\partial n/\partial x_i\,(x,y,z)$ that correspond to the measured background displacements and associated ray deflections will be performed using either Fourier slice based filtered back projection (FBP) [6], iterative algebraic reconstruction techniques (ART) [7] or a combination of both.

3.1 Filtered Back Projection (FBP)

In the present implementation the reconstruction of each refractive index gradient is performed independently based on sinograms that represent the sum of each component of $\sum_{ray}\nabla n$ along the camera's axis at each position along the width of each camera. The sum of the gradients at each position in the image plane are determined by solving the following system of equations:

$$\frac{n_o}{\Delta x}\begin{bmatrix}\varepsilon_{x'}\\ \varepsilon_{y'}\\ \varepsilon_{z'}\end{bmatrix} = \begin{bmatrix}\mathbf{x}'^T\\ \mathbf{y}'^T\\ \mathbf{z}'^T\end{bmatrix}\sum_{ray}\nabla n \tag{5}$$

where n_o is the refractive index outside the measurement volume and Δx is the voxel width. Reconstruction is performed following the common practice of taking the inverse Radon transform of ramp filtered sinograms. A circular reconstruction domain is applied which corresponds to the common view of all cameras, outside which the density gradients are set to zero.

3.2 Algebraic Reconstruction Technique (ART)

The algebraic density gradient reconstruction is based on representing the defection angles $\varepsilon_{x'i}$, $\varepsilon_{y'i}$, $\varepsilon_{z'i}$ for the i-th ray as a projection of the gradients of the refractive index field ∇n where the contribution of each j-th point in the field is represented by a weighting w_{ij}. From equations (3) and (4) the contribution to the ray deflections can be expressed as:

$$\varepsilon^k_{x'i} = L_i\frac{\sum_j w_{ij}\mathbf{x}'\cdot\nabla n^k_j}{n_o\sum_j w_{ij}} \qquad \varepsilon^k_{y'i} = L_i\frac{\sum_j w_{ij}\mathbf{y}'\cdot\nabla n^k_j}{n_o\sum_j w_{ij}} \qquad \varepsilon^k_{z'i} = L_i\frac{\sum_j w_{ij}\mathbf{z}'\cdot\nabla n^k_j}{n_o\sum_j w_{ij}} \tag{6}$$

where k denotes the iteration of the reconstruction and L_i is the length of the path followed by the ray through the volume. A solution to the gradient field is computed by iteratively correcting a previous estimation of the field in order to minimise the difference between the projected deflection angles of each ray as calculated by equation (6) and the deflection angles estimated from the measured background displacements, equation (4). The required correction for each gradient component is determined by solving the following series of equations,

$$\frac{\lambda_j n_o w_{ij}}{L_i}\begin{bmatrix}\varepsilon_{x'i}-\varepsilon^k_{x'i}\\ \varepsilon_{y'i}-\varepsilon^k_{y'i}\\ \varepsilon_{z'i}-\varepsilon^k_{z'i}\end{bmatrix} = \begin{bmatrix}\mathbf{x}'^T\\ \mathbf{y}'^T\\ \mathbf{z}'^T\end{bmatrix}\left(\nabla n^{k+1}_j - \nabla n^k_j\right) \tag{7}$$

where λ_j is a relaxation parameter set to 2.0 through this paper.

3.3 Calculation of the Refractive Index Field

The refractive index fields $n(x, y, z)$ can be calculated from their reconstructed gradients by solving the Poisson equation:

$$\nabla^2 n = \frac{\partial^2 n}{\partial x^2}+\frac{\partial^2 n}{\partial y^2}+\frac{\partial^2 n}{\partial z^2} = q \tag{8}$$

The right-hand side is populated by taking a 2^{nd} order central difference of the reconstructed density gradients with the solution obtained via an iterative successive over relaxation algorithm (SOR). In the present case the solution was terminated once the field had converged to 10^{-16}, to remove any influence of the convergence of the SOR algorithm on the assessment of the reconstruction methodology. As is often done in PIV a lower order discretisation is to reduce the influence of measurement and reconstruction noise associated with the gradient fields.

4 Generation of Synthetic Backgrounds

To assess the performance of the proposed reconstruction methods synthetic BOS images were created by tracing rays from each camera through a known refractive index distribution using Snell's law. A synthetic field consisting of a Gaussian air jet with a peak change in refractive index of $\Delta n_p = 1.5\times10^{-4}$ from $n_0 = 1.0$ was used, corresponding to a centreline temperature of approximately 368˚C at standard atmospheric conditions, and a standard deviation σ = 9 voxels. The measurement domain of 65×3×65 voxels (43×2×43 mm) was sized based on a jet diameter of 10 mm and the use of a 1 Mpixel camera with a pixel size of 3.75×3.75 µm^2 equipped with f = 25 mm focal length lens with an aperture of f/22. The optical centre of the camera was positioned 275 mm from the centre of the volume and 575 mm from the background so that an interrogation window of 16 pixels would correspond to 16 voxels (0.66 mm) when projected to the volume centre and remain larger than the circle of confusion associated with the lens geometry of the BOS setup (see [8] for a discussion of the influence of finite aperture on BOS).

Synthetic background images were created for different camera numbers, with cameras evenly spaced in a 180◦ arc about the jet axis in the *x-z* plane (see Fig. 2). Such a camera configuration is relatively practical to setup, lends itself well to FBP and results in reconstruction that is almost independent of variation in the *y−axis*. This allows us to perform a more efficient comparison of the different reconstruction methods by limiting our region of interest to a thin slice normal to the jet axis.

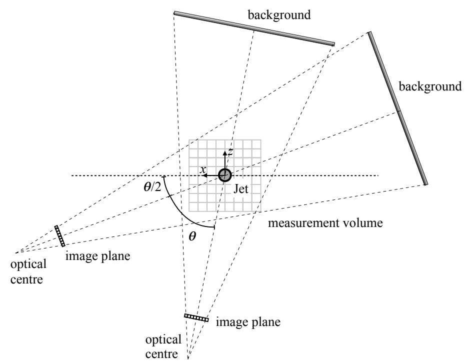

Figure 2: Schematic of the synthetic BOS configuration

To assess the ability of TBOS to resolve instantaneous turbulent density fluctuations, the Gaussian refractive index distribution was modulated using sinusoids in the *x* and *z* directions as given by:

$$n(x,y,z) = \frac{1}{2\pi\sigma^2} e^{-[x^2+z^2]/(2\sigma^2)} \left[1 + A\sin\left(\frac{2\pi}{\lambda_x}x\right)\sin\left(\frac{2\pi}{\lambda_x}z\right)\right] \qquad (9)$$

where λ_x and λ_z are wavelengths of density fluctuations, A is the amplitude of the modulation, which was set to 0.25 such that the field consists of fluctuations up to 25% of the mean value, which decay towards the jet boundaries. This is similar to passive scalar fluctuations in a fully developed turbulent round jet [9]. The maximum background displacements in the image plane were 1 pixel.

5 Results

To assess the ability of the TBOS algorithms to resolve instantaneous density and corresponding refractive index fluctuations noiseless background displacement fields were generated for arrays of 6 to 22 evenly spaced cameras, with fluctuation wavelengths from $\lambda_x = \lambda_y = 4.6$ to 32.5 voxels or $L/14$ to $L/2$ where L is the measurement volume length.

Simulations showed that ART performed best when iterative corrections to the density field were performed by randomly sampling rays from each camera, which removes bias to any particular image, combined with a masking of the gradient field beyond a radius of 30 voxels and imposing a Hamming window to the correction, which similarly reduces the correction applied to the outer region of the reconstruction domain. As shown in Fig. 3, FBP provides a good reconstruction of gradients near the centre of the volume but also introduces considerable gradients outside the core of the

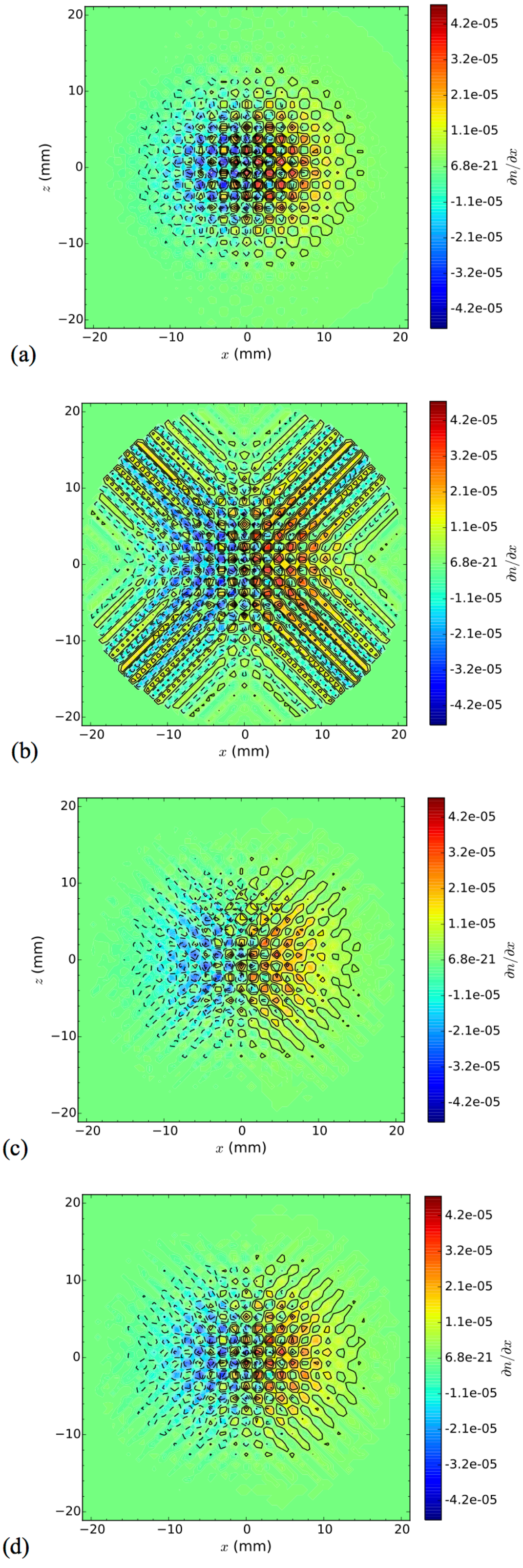

Figure 3: Contour plots for the reconstructed refractive index gradient $\partial n/\partial x$ for 14 cameras and $\lambda_{x,y} = L/14$: (*a*) synthetic field; (*b*) FBP; (*c*) ART 20 iteration; and (*d*) FBP+ART 10 iterations.

synthetic jet. Removing these regions then applying an ART reduces the sensitivity to the applied mask and in all cases converged to a solution better than that of ART alone by maintaining the strong gradients near the centre of the volume. ART with a null initial gradient field tends to under-predict the gradients near the centre of the volume and require approximately twice as many iterations to reach the same convergence.

The accuracy of a TBOS computed refractive index field depends not only on the reconstruction methodology but also on the number of the background views, the strength of the density gradients and the relative distance between the volume and the background. The influence of the number of cameras and the wavelength of the oscillation in the refractive index field for the FBP+ART reconstructions is demonstrated in Fig. 4 assuming exact calculations of the background displacement. A range of 6 to 22 cameras was considered as less camera results in significant errors and the benefit associated with the use of more cameras drops off significantly.

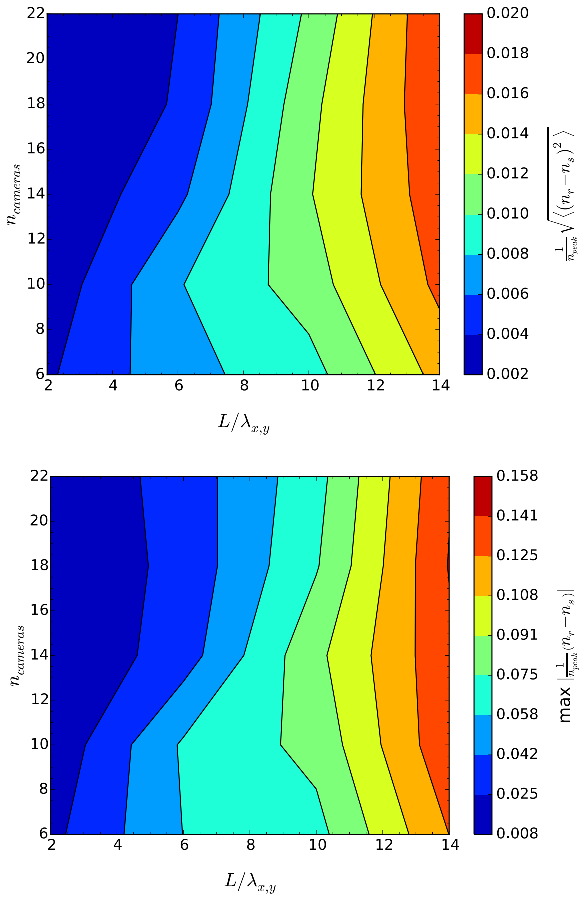

Figure 4: Contour maps of the RMS and peak errors between the synthetic and computed refractive index fields normalised by the peak refractive index gradient from Poisson solution with refractive index gradients computed by FBP+ART 10 iterations.

In all cases reducing the wavelength of the density oscillations significantly increases both the RMS and peak errors in the reconstructed fields when compared to the synthetic field. The extent to which the magnitude of these errors are influenced by spatial resolution is still under investigation. Comparison of the different reconstruction methods shows that FBP+ART provides the most accurate estimate of the refractive index field across the entire range of wavelengths. Increasing the number of cameras improves the reconstruction, however the benefit beyond the use of 18 cameras is almost negligible. This suggests that high quality TBOS measurements of turbulent flows will likely require between 16 to 18 cameras. It is important to note that unlike PIV cameras the cameras used for BOS do not have to operate in a double shutter mode, allowing for the use of lower cost machine vision cameras. While results indicate that the mean reconstruction error across the field is relative small, the reconstruction in unable to accurately predict the strongest small scale gradients resulting in peak errors of up to 15% of the peak.

4 Conclusions

The ability of a tomographic background oriented schlieren technique to reconstruct a fluctuating density field of differing scales and camera number is assessed using filtered back projection, algebraic reconstruction and a combination of the two. In all cases, using the filtered back projection as an initial solution to the algebraic solution was found to yield the best reconstruction of both the core of the heated jet and the flow boundaries. The accuracy of the reconstruction is strongly affected by the scale of the density fluctuations. Attempts to improve the effective resolution of such measurements is currently underway.

5 Acknowledgment

The support of Australian Research Council (ARC) for this work is gratefully acknowledged, Dr. Atkinson was supported by an ARC Discovery Early Career Researcher Award (DECRA) fellowship while undertaking this work.

References

[1] G. Elsinga,, F. Scarano, B. Wieneke, B. van Oudheusden, Experiments in Fluids 41(6) (2006) 933–947

[2] C. Atkinson, J. Soria, Experiments in Fluids 47(4) (2009) 553–568

[3] G. Meier, Experiments in Fluids 33 (2002) 181-187

[4] B. Atcheson, I. Ihrke, W. Heidrich, A. Tevs, D. Bradley, M. Magnor, H.P. Seidel, Proc. ACM transactions on graphics (TOG), ACM, vol 27 (2008) 132-

[5] E. Goldhahn, J. Seume, Experiments in Fluids 43(2-3) (2007) 241-249

[6] A. C. Kak and M. Slaney, Principles of Computerized Tomographic Imaging, IEEE Press, 1988

[7] G.T. Herman, A. Lent, Computers in biology and medicine 6(4): (1976) 273– 294

[8] H. Richard, M. Raffel, Measurement Science and Technology 12(9) (2001) 1576

[9] N. Panchapakesan, J. Lumley, Journal of Fluid Mechanics 246 (1993) 225–247